J. Fluid Mech. (1983), *vol.* 127, *pp.* 443–452
Printed in Great Britain

Drag-force fluctuation on a cylinder

By R. SHEDDEN AND S. P. LIN
Clarkson College of Technology, Potsdam, New York 13676

(Received 25 September 1981 and in revised form 7 September 1982)

The drag force acting on a circular cylinder fluctuating erratically in a viscous fluid is measured with a laser–cantilever force transducer. The experimental results compare very well with the theory.

1. Introduction

The most extensively studied unsteady flow about a cylinder is probably that created by a circular cylinder that is impulsively set to a constant-velocity translation. Coutanceau & Bouard (1977) and Bouard & Coutanceau (1980) have made detailed experimental investigations of the time evolution of the boundary-layer separation and the symmetric wake regions in such a flow. They compared their observations, favourably in general, with the theoretical predictions cited in their works. These theoretical works are based either on the boundary-layer approximation or on the direct numerical integration of the Navier–Stokes equation at moderate values of the Reynolds number. At higher Reynolds numbers asymmetric vortex shedding occurs, and the resulting flow fields become more complex. Nevertheless, these complex flows have also been studied extensively because of their importance in various applications including flow-induced structural vibration and acoustics (see e.g. Phillips 1956). Interesting reviews on the subject are given by Berger & Wille (1972) and Sarpkaya (1979). Three-dimensional separated flows are reviewed by Tobak & Peake (1982).

Less well studied unsteady flows about a cylinder are those that involve neither vortex shedding nor sustained boundary-layer separation. Such flow can be created, for example, by a high-frequency small-amplitude fluctuation of a body in an initially quiescent fluid. If the typical period of the cylinder fluctuation is much shorter than the time required for maintaining the integrity of a boundary-layer structure, the flow separation cannot be sustained nor can the vortex shedding ensue. For this class of highly transient flows the boundary-layer approximation is inadequate, but the solution of the unsteady Stokes equation can be used to start the successive approximate solution of the Navier–Stokes equation. A bounded solution of the unsteady Stokes equation was obtained by Lin (1975) for the flow created by an erratically fluctuating cylinder in his study of the damped vibration of a string. The results were applied by Lin & Gautesen (1976) to determine the transient initial drag on a cylinder starting an arbitrary acceleration from rest. The method was extended by Lin (1980) in his study of the migration of the separation point and the transient heat transfer from a hot film. The general analytical solution obtained with an unconventional method by Lin & Gautesen recovers, as special cases, the known solutions for flows created by a cylinder that undergoes some certain prescribed motions. However, their theory has not yet been confirmed by experiments. This work reports an experiment on the fluctuation of drag force on a cylinder, which agrees with the theory. As far as we are aware, this is the first experimental study of the drag fluctuation in a flow regime described earlier in this paragraph.

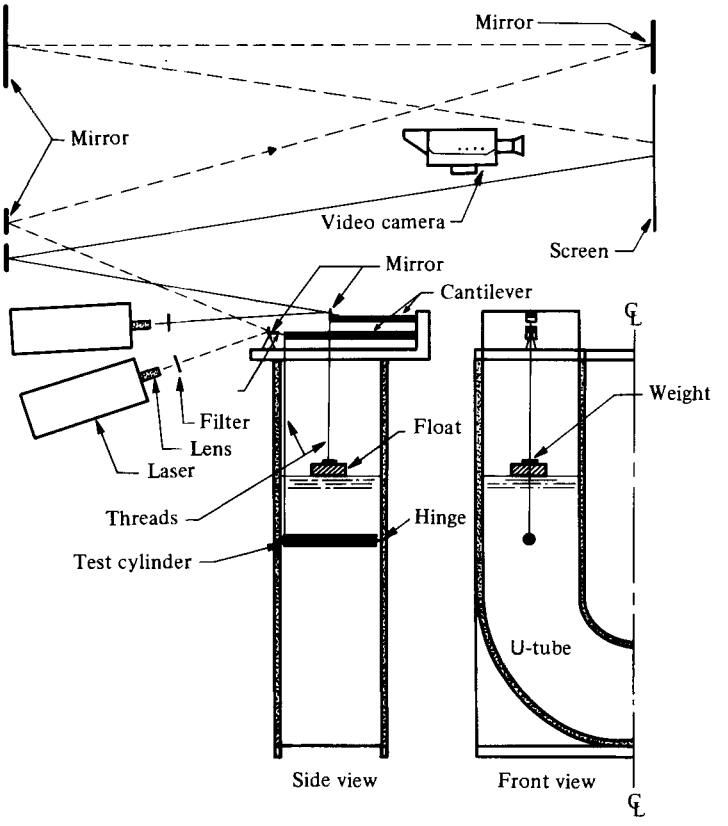

FIGURE 1. Experimental set-up.

2. Theoretical background

The drag force D on a cylinder fluctuating erratically in a direction normal to the axis is, to the first-order approximation given by Lin (1975),

$$D = \pi L\rho\nu U\left[\dot{V} + \frac{16}{\pi^2}\int_0^\tau\int_0^\infty \dot{V}(\lambda)\frac{\exp[-S^2(\tau-\lambda)]}{S[J_0^2(S)+Y_0^2(S)]}dS\,d\lambda\right]$$

$$= \pi L\rho\nu U\left[\dot{V} + 4\int_0^\tau \dot{V}(\lambda)\{\pi(\tau-\lambda)\}^{-\frac{1}{2}}d\lambda + 2\{V(\tau)-V(0)\}\right.$$

$$\left. -\pi^{\frac{1}{2}}\int_0^\tau \dot{V}(\lambda)(\tau-\lambda)^{\frac{1}{2}}d\lambda + \frac{1}{2}\int_0^\tau \dot{V}(\lambda)(\tau-\lambda)\,d\lambda + O(\tau^{\frac{3}{2}})\right] \quad (\tau \ll 1), \tag{1}$$

where L is the length of the test cylinder, ρ and ν are respectively the density and viscosity of fluid, V is the cylinder velocity non-dimensionalized with its maximum velocity U, the upper dot denotes differentiation with respect to dimensionless time τ defined by $\tau = t/(a^2/\nu)$, a and t being respectively the cylinder radius and time, and J_0 and Y_0 denote the zeroth-order Bessel functions of the first and second kind respectively. Equation (1) is valid in a highly fluctuating flow such that the typical frequency ω and amplitude ϵ of the fluctuation satisfy the conditions

$$\nu \ll d^2\omega, \quad \epsilon \ll d, \tag{2}$$

where $d = 2a$. The truncation error involved in (1) is $O(\epsilon)$.

In the present work both D and $\dot{V}$ will be determined experimentally. D can also be calculated from (1) with the measured $\dot{V}$ as input. The theoretical values of D will be compared with that obtained experimentally.

3. Experimental technique

The general layout of the experiment is shown in figure 1. A Plexiglas tank standing 100 cm tall was formed in the shape of a U-tube with a 20·1 cm square cross-section. Water, which was the only test fluid used, was filled to different levels to produce different frequencies of flow oscillation. Different amplitudes of flow fluctuation were produced by raising the water level in one leg of the U-tube, with a piston or compressed air pressing down on the water surface in the other leg, and then suddenly releasing the pressure. The drag force exerted by the subsequent fluctuating flow on a test cylinder submerged in the U-tube is of central interest in this experiment. The methods of measurements of the instantaneous drag force and the corresponding relative velocity of the cylinder to the ambient fluid are described in §§3.1 and 3.2.

3.1. *Drag force*

One end of a 20 cm long test cylinder was mounted on a hinge fastened on a vertical wall of the U-tube as shown in figure 1. The other end was suspended by a thread, which was connected to the free end of a 0·32 × 0·32 × 30 cm cantilever beam mounted on a platform fastened to the rim of the U-tube. The cylinder was at least 14 diameters below the water surface, and was horizontal before the flow oscillation was introduced. The drag fluctuation on the cylinder is only a small fraction of the tensile force in the thread, and thus the suspending thread was always taut. The instantaneous drag on the cylinder was linearly related to the small displacement of the free end of the cantilever. The displacements were so small that accurate measurements were not possible without amplifying them. A 0·635 cm square mirror was attached to a metal pivot fulcrum. On the opposite end of the pivot plate a small hinge was connected to the cantilever. A 5 mW laser beam was aimed at the mirror and then reflected several times as shown in figure 1 before reaching a graph screen on which a small displacement of the free end of the cantilever was translated into an appropriately magnified displacement of the laser-beam image. To calibrate the cantilever displacement with that of the laser beam on the screen, a dial gauge with an uncertainty of 0·000254 cm was solidly mounted above the cantilever beam. The gauge point was in contact at the same point at which the thread was connected. A displacement of the cantilever is induced manually and its magnitude read directly from the gauge. The corresponding displacement of the laser beam was read directly off the graph screen. A set of these two readings form the calibration curve, which is shown in figure 2. This curve will be used later to determine the ambient fluid velocity.

To obtain the calibration curve for the drag force on the cylinder, small known weights are placed on the cylinder at its centre, and the corresponding displacements of the laser beam on the screen are recorded. A set of these data points is also given in figure 2.

For each experiment the time history of the laser-beam displacement on the screen was recorded by use of a videotape system set up to photograph at 60 frames per second. The camera was a Sony black and white camera with $f/1{\cdot}8$ normal lens. The recorded tape was then transferred to a Sony reel-to-reel deck so that each frame could be observed individually and the displacement at any time measured. The recorded displacements were translated into the time histories of the drag force and the displacement of the free end of the cylinder by use of the respective calibration

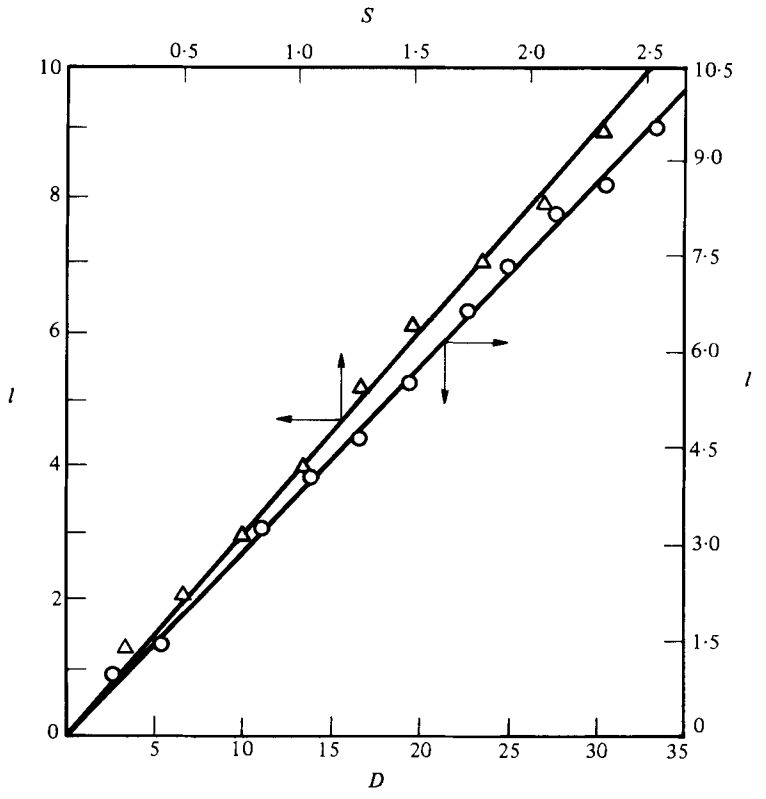

FIGURE 2. △, Calibration curves of the force transducer used for a Plexiglas test cylinder of 1·27 cm diameter: ○, experimental points; ——, least-square fit; l, displacement of laser beam image in cm; S, displacement of the free end of cylinder in 10^{-3} cm; D, drag force in 10^{-5} N.

curves just described. Note that the displacements of the free ends of the cantilever and the cylinder are essentially the same since the variation in the length of the connecting thread is negligibly small owing to the fact that the maximum drag force is at most only 2% of the tensile force in the thread.

3.2. *Fluid velocity*

To determine the velocity of the cylinder relative to the ambient fluid, we first recorded the instantaneous position of the free surface above the test cylinder. A 5 cm tube of styrofoam of density 0·03 gm/cm^3 was suspended by a thread attached to the free end of a 0·32 × 0·32 × 20 cm cantilever beam, which was mounted over the U-tube as shown in figure 1. A small weight was placed on the float such that when the free-surface level was at its lowest during the experiment the float was still in contact with the free surface, and when the water level is at its highest level the thread was still in high tension. As the free surface fluctuates, the float responds instantly with little inertial effect. Thus the float fluctuation was taken to be the same as the free-surface fluctuation which was transmitted through the high-tension thread attached to the cantilever sensor. Again, the signal at the sensor must be amplified for accuracy. The methods of signal amplification and the displacement-sensor calibration as well as the method of recording the free surface displacement were identical with those used in §3.1, and need not be repeated here. The calibration curve for the free-surface displacement is given in figure 3. By use of this curve, the

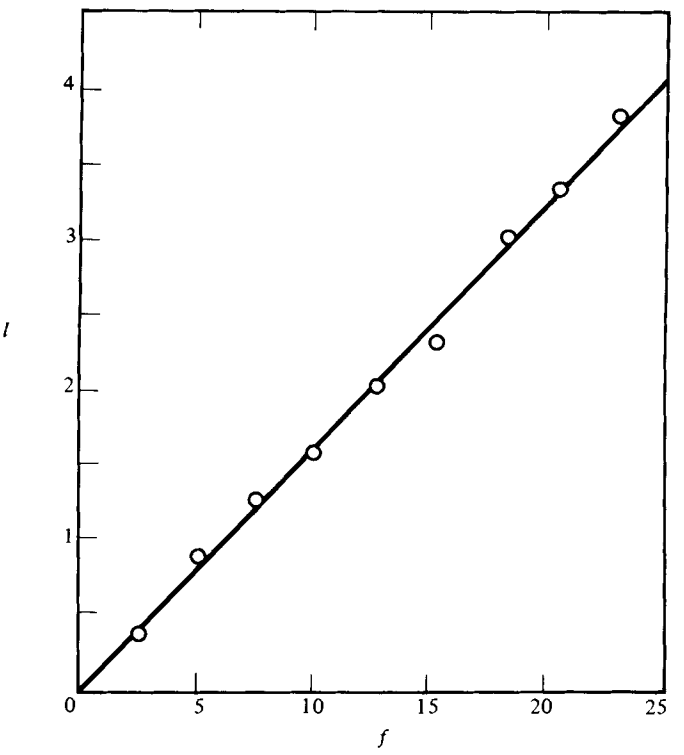

FIGURE 3. A calibration curve for the measurement of water free surface in the U-tube: ○, experimental points; ——, least-square fit; l, displacement of laser-beam image in cm; f, displacement of the free surface in 10^{-2} cm.

free-surface displacement can be plotted as a function of time from the recorded data. The time differentiation of this plot gives the instantaneous free-surface velocity. Similarly the time differentiation of the plot of the cylinder displacement *versus* time described in §3.1 gives the velocity of the free end of the test cylinder. One-half of this velocity is the average velocity of the cylinder. The average cylinder velocity is at most 2 % of the corresponding free-surface velocity in our experiments. To obtain the ambient fluid velocity with respect to the cylinder, we subtracted or added the average cylinder velocity to the free-surface velocity, depending on the direction of the displacements relative to each other. The velocity V appearing in (1) therefore is equal in magnitude but opposite in direction to the ambient fluid velocity thus determined divided by the maximum velocity in each experiment.

4. Results

Two test cylinders were used. The first one was a hollow plastic cylinder of 0·635 cm outside diameter and 0·318 cm inside diameter. The second one was a 1·27 cm diameter solid Plexiglas cylinder. The time records of the relative displacement with respect to the ambient fluid are first plotted. The graphical time differentiation of each displacement curve then gives the relative velocity. The velocity curves thus obtained are normalized with the maximum velocity in each curve and plotted against the dimensionless time τ in figures 4(*a*) and 5(*a*). The displacement curves are also recorded in these figures for reference. As can be seen from these figures, the

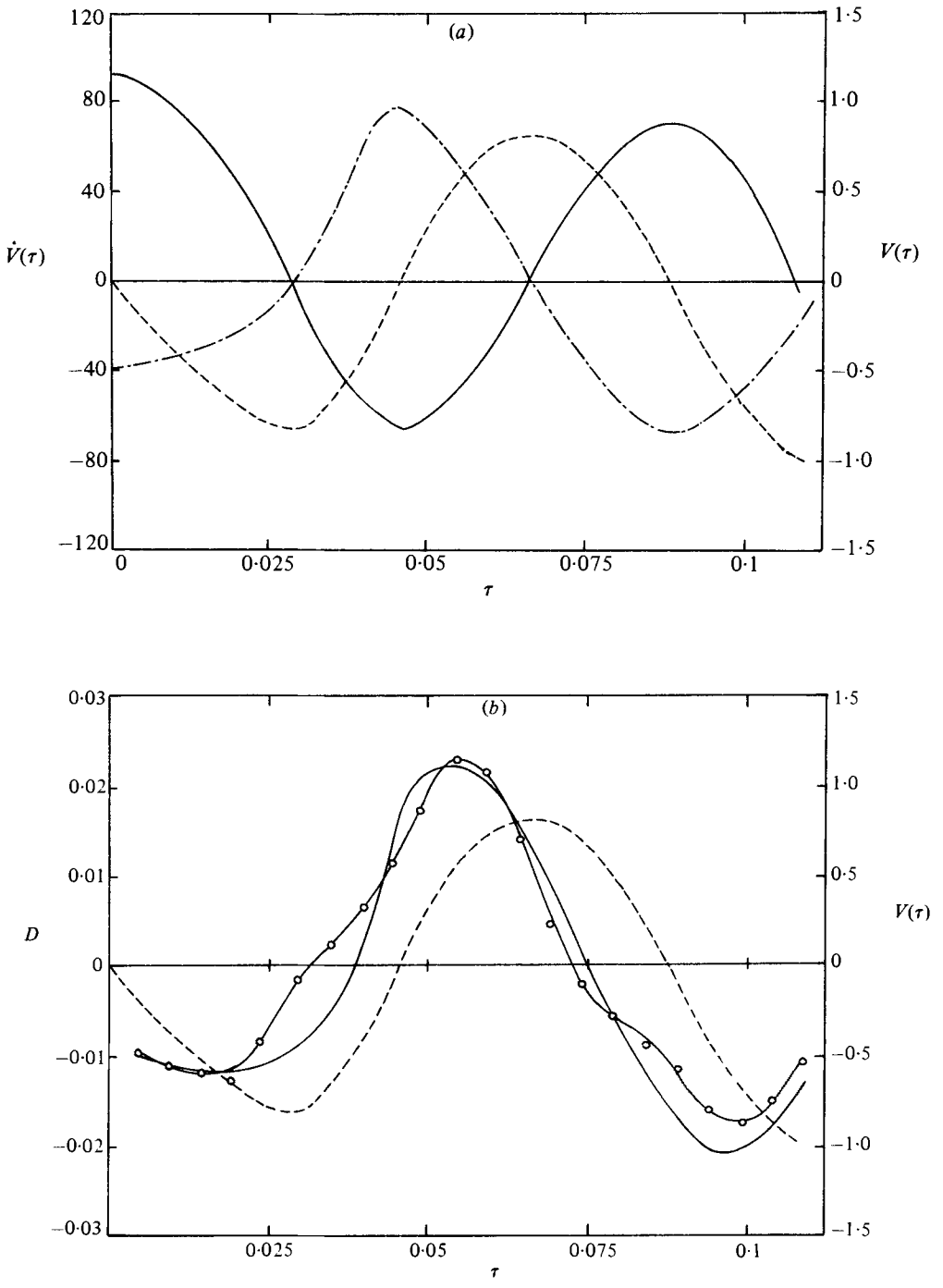

FIGURE 4. Results for a hollow plastic cylinder of 0·635 cm outside diameter. (*a*) ——, displacement; ---, velocity; ———, acceleration; displacements in cm = acceleration scale × 3·175 × 10^{-3}. (*b*) –○–, experimental drag; ——, theoretical drag; ----, $V(\tau)$; drag force in N.

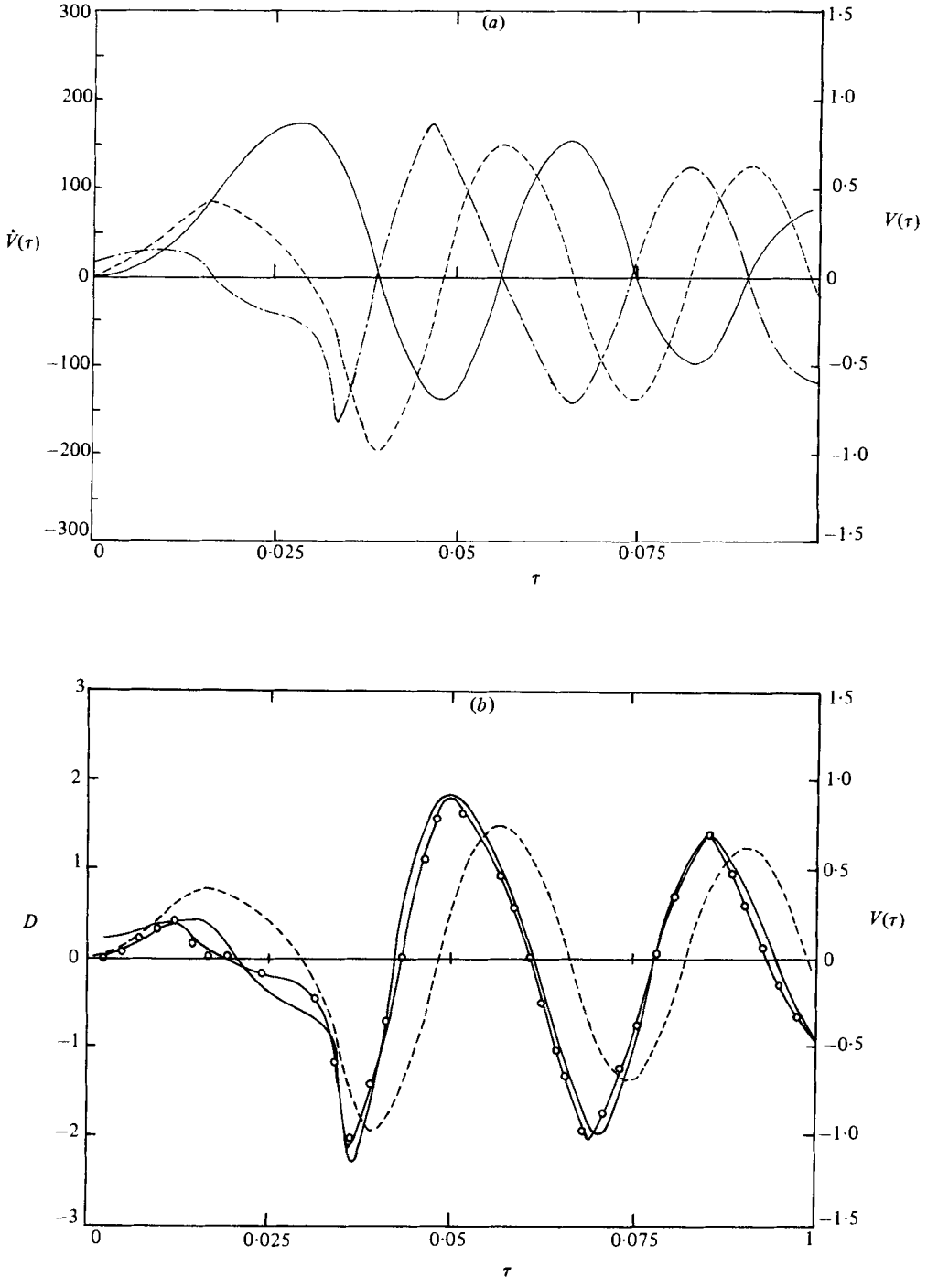

FIGURE 5. Results for a solid Plexiglas cylinder of 1·27 cm diameter. (*a*) ——, displacement; ----, velocity; – – –, acceleration; displacement in cm = acceleration scale $\times 2{\cdot}54 \times 10^{-4}$. (*b*) –○–, experimental drag; ——, theoretical drag; ----, $V(\tau)$; drag force in 10^{-4} N.

relative velocities of the cylinder to fluid are not sinusoidal. The acceleration curves in these figures were obtained by graphical time differentiation of the velocity curves. Substituting the velocity and acceleration of each cylinder into the right-hand side of (1) and carrying out the numerical integration by the Gauss quadrature, we obtained the respective drag force. The test fluid was water at 20 °C with $\rho = 1$ g/cm^3 and $\nu = 0{\cdot}01$ cm^2/s. Calculated drag forces as functions of time are given in figures 4(*b*) and 5(*b*) together with the measured values. The corresponding cylinder velocity curves are also given in the same figures to show the time lag of the drag force behind the velocity. It is easily seen from figure 4(*a*) that the dimensionless period of the first cycle of fluctuation is approximately 0·088. The corresponding dimensional period, frequency and amplitude are respectively 0·89 s, $7{\cdot}08/2\pi$ Hz and 0·29 cm. Thus, while the first condition in (2) was amply satisfied, the second one in (2) was not satisfied since $\epsilon \sim 0{\cdot}9$. The Reynolds number $Re \equiv \omega\epsilon d/\nu$ for this experiment was 128·5. Similarly, it was found from figure 5(*a*) that the characteristic frequency and amplitude of the flow fluctuation in the second experiment were respectively 3·7 rad/s and 0·045 cm. The corresponding Reynolds number is 21. It is easily verified that both conditions in (2) are amply satisfied. This explains why the second experiment found better agreement with the theory than the first one.

According to the error analysis given in §5, the error bounds on the measurements of the displacement, velocity, dimensionless velocity, dimensionless acceleration and drag force are respectively 0·017 cm, 0·11 cm/s, 0·05, 1·4 and $1{\cdot}34 \times 10^{-5}$ N for the case of $d = 0{\cdot}635$ cm. The corresponding error bounds for the case of $d = 1{\cdot}27$ cm are respectively 0·0163 cm, 0·034 cm/s, 0·142, 2·97 and $4{\cdot}1 \times 10^{-6}$ N.

5. Error analysis

Experimental error bounds on the measured displacement, velocity, acceleration and drag force will now be given. Consider first the case of $d = 0{\cdot}635$ cm. It is obtained from figure 3 that $df/dl = 0{\cdot}0625$. The maximum error of reading the laser-beam image on the screen is estimated to be 0·1 cm. Thus the error on the free-surface displacement due to the reading error is $0{\cdot}1 \times 0{\cdot}0625 = 6{\cdot}25 \times 10^{-3}$ cm. The error of constructing the calibration curve (f, l) itself is two orders of magnitude smaller than this. The error in the free-surface displacement relative to the cylinder due to the elongation or contraction of the cotton thread of 0·01 cm diameter which is attached to the free end of the test cylinder is 7×10^{-4} cm. This estimate is based on the Young's modulus of $6{\cdot}5 \times 10^{10}$ N/m^2 (Baumeister 1967) and the maximum drag force on the 20 cm cylinder being 0·023 N. It was assumed in the free-surface-displacement measurements that there is no relative motion between the free surface and the float. In order to test this assumption, we photographed the motions of the free surface and the float on a videotape with the aid of a microscope. The results were analysed on the TV screen. It was found that the float and the free surface have an identical period of oscillation with a maximum error of $\frac{1}{60}$ s. Within the space resolution of 0·01 cm, no motion of the float relative to the free surface can be detected. The buoyant force corresponding to this maximum undetectable displacement of 0·01 cm is $2{\cdot}45 \times 10^{-3}$ N, which is one order of magnitude smaller than the drag force acting on the test cylinder. Therefore the maximum extension or contraction of the thread connecting the float and the displacement transducer is 7×10^{-5} cm, being approximately $\frac{1}{10}$ of that connecting the test cylinder and the force transducer. Thus we conclude that the maximum displacement of the float relative to the free surface is

less than 0·01 cm. The error associated with the measurement of the displacement of the test cylinder can be estimated as $(dS/dl)\,\Delta l$. According to figure 2, $dS/dl = 2{\cdot}2 \times 10^{-4}$, and the laser-beam-image reading accuracy is $\Delta l = 0{\cdot}1$ cm. Therefore $(dS/dl)\,\Delta l = 2{\cdot}2 \times 10^{-5}$ cm. Hence the total error bound on the displacement of the test cylinder relative to the fluid is $1{\cdot}7 \times 10^{-2}$ cm. The typical displacement used in constructing the slope of the displacement curve was 0·545 cm. The corresponding time interval is 0·252 s. The angle resolution in the slope construction was 1°. Thus the error on velocity due to the limited angle resolution is $(\pi/180) \times (0{\cdot}545/0{\cdot}252) = 3{\cdot}78 \times 10^{-2}$ cm/s. The error on velocity due to the above-mentioned error in displacement is $0{\cdot}017/0{\cdot}252 = 0{\cdot}068$ cm/s. The time resolution available in the numerical differentiation of the displacement curve was $\frac{1}{30}$ s. Thus the error due to the limited time resolution is $\frac{1}{30}(0{\cdot}038 + 0{\cdot}068) = 0{\cdot}0035$ cm/s. The total error bound on velocity is therefore 0·1095 cm/s. The corresponding dimensionless velocity resolution in figure 4 is 0·05. The dimensionless acceleration was obtained by graphically differentiating the dimensionless velocity curve. The maximum slope encountered was 80. The resolution on the angle reading is 1°. Therefore the resolution on the dimensionless acceleration is $(\pi/180) \times 80 = 1{\cdot}4$. The dimensionless time resolution available was $2{\cdot}5 \times 10^{-4}$. The error due to time reading is therefore two orders of magnitude smaller than that due to angle reading. According to figure 2, $dD/dl = 3{\cdot}3 \times 10^{-3}$ N/m. The uncertainty involved in reading the laser-beam image is 0·1 cm. The corresponding error in drag force is $(dD/dl)\,\Delta l = 3{\cdot}34 \times 10^{-6}$ N. The drag force acting on the free end of the test section can be estimated to be 7×10^{-7} N, by use of the Couette-flow formula. The required input data are $d = 0{\cdot}635$ cm, the gap between the U-tube wall and the cylinder is 0·01 cm, the maximum relative velocity of fluid to the cylinder is $U_m = 2{\cdot}16$ cm/s, the fluid viscosity is $\mu = 0{\cdot}01$ g/cm s. The viscous drag on the hanging thread is $\mu L U_m = 6{\cdot}5 \times 10^{-6}$ N (Brenner 1962), where $L = 30$ cm is the thread length. The friction exerted by the pin at the force transducer is estimated to be $1{\cdot}4 \times 10^{-6}$ N, by use of the circular-Couette-flow formula. Similarly the friction exerted by the pin at the hinge on the test cylinder is found to be $1{\cdot}4 \times 10^{-8}$ N. The latter friction is smaller than the former one, because the rotational velocity at the hinge is two orders of magnitude smaller than that at the pin on the force transducer. The total error bound on drag is therefore $1{\cdot}34 \times 10^{-5}$ N.

The error analysis for the case of $d = 1{\cdot}27$ cm follows the same line. The errors associated with reading the image on the screen and the error due to the inertia of float remain the same. The error due to the elongation or contraction of the thread attached to the test cylinder is $\frac{1}{100}$ of that in the previous case, since the maximum force in the thread is slightly more than 100 times as small. Hence the total error on the displacement of the cylinder relative to the fluid is $1{\cdot}63 \times 10^{-2}$ cm. The typical displacement used in constructing the slope of the displacement curve was 0·121 cm. The corresponding time interval is 0·504 s. Thus the error in velocity due to the limited angle resolution of 1° is $(\pi/180)\ (0{\cdot}121/0{\cdot}504) = 4{\cdot}19 \times 10^{-3}$ cm/s. The error in velocity propagated from the displacement error is $0{\cdot}0163/0{\cdot}504 = 0{\cdot}032$ cm/s. The error in velocity due to the limited time resolution of $\frac{1}{30}$ s is $\frac{1}{30} \times (0{\cdot}0042 + 0{\cdot}032) = 0{\cdot}0012$ cm/s. The total error bound on velocity is 0·034 cm/s. The corresponding dimensionless velocity resolution in figure 5 is 0·14. The resolution on the dimensionless acceleration is $(\pi/180) \times 170 = 2{\cdot}97$. The ratios of the diameter and velocity of the present case to that of the previous case are respectively (1·27/0·635) and (0·24/2·16). Hence the neglected drag force acting on both ends of the test section is less than $2 \times (1{\cdot}27/0{\cdot}635)^2\ (0{\cdot}24/2{\cdot}16) \times 7 \times 10^{-7}$ N $= 6{\cdot}2 \times 10^{-7}$ N. The viscous drag

on the hanging thread is 0·24/2·16 times that of the previous case. The same multiplication factor applies to the friction forces on the pin and hinge described in the previous case. The largest error on drag force is due to reading error, which was found to be $3{\cdot}34 \times 10^{-6}$ N. Hence the total error bound on drag force for this case is $4{\cdot}1 \times 10^{-6}$ N.

Finally we note that most of the drag forces reported in this experiment were too small to be measured by standard methods of force transduction such as strain gauges due to electrical noise and radio-frequency interference, which was of the same order of magnitude as the drag-force readings. Moreover, the present results on instantaneous velocity cannot be obtained with a hot wire or a hot film, because their calibrations are based on an assumption that the relative fluid velocity and the associated heat transfer they detect are always in phase. This assumption is not valid in the highly transient situation considered in our work.

This work was supported in part by a National Science Foundation Grant ENG 79-02870. R. Shedden was supported by an Alcoa Fellowship. Thanks are due to Mr C. Aidun for his assistance on the ciné microphotography used in the last phase of the experiment.

REFERENCES

Bouard, R. & Coutanceau, M. 1980 The early stage of development of the wake behind an impulsively started cylinder for $40 < Re < 10^4$. *J. Fluid Mech.* **101**, 583.

Berger, E. & Wille, R. 1972 Periodic flow phenomena. *Ann. Rev. Fluid Mech.* **4**, 313.

Baumeister, T. 1967 *Handbook for Mechanical Engineers*, 7th edn, p. 6–184. McGraw Hill.

Brenner, H. 1962 Effect of finite boundaries on the Stokes resistance of an arbitrary particle. *J. Fluid Mech.* **12**, 35.

Coutanceau, M. & Bouard, R. 1977 Experimental determination of the main features of the viscous flow in the wake of a circular cylinder in uniform translation. Part 2. Unsteady flow. *J. Fluid Mech.* **79**, 257.

Lin, S. P. 1975 Damped vibration of a string. *J. Fluid Mech.* **72**, 787.

Lin, S. P. 1980 Transient momentum and heat transfer from a cylinder. *Arch. Mech.* **32**, 831.

Lin, S. P. & Gautesen, A. 1976 Initial drag on a cylinder. *Q. J. Mech. Appl. Math.* **29**, 61.

Phillips, O. M. 1956 The intensity of Aeolian tones. *J. Fluid Mech.* **1**, 607.

Sarpkaya, T. 1979 Vortex induced oscillations. *Trans. A.S.M.E.* E: *J. Appl. Mech.* **46**, 241.

Shedden, R. 1980 Transient drag on a cylinder. M.S. thesis (*Tech. Rep.* MIE-060), Clarkson College of Technology, Potsdam, N.Y. 13676.

Tobak, M. & Peake, D. J. 1982 Topology of three-dimensional separated flows. *Ann. Rev. Fluid Mech.* **14**, 61.